Draft version April 27, 2020
Typeset using LaTeX default style in AASTeX63

Calibrating gyrochronology using Galactic kinematics

Ruth Angus,[1,2,3] Yuxi (Lucy) Lu,[3,1] Dan Foreman-Mackey,[2] Adrian M. Price-Whelan,[2] Jason Curtis,[1] and Emily Cunningham[2]

[1]*Department of Astrophysics, American Museum of Natural History, 200 Central Park West, Manhattan, NY, USA*
[2]*Center for Computational Astrophysics, Flatiron Institute, 162 5th Avenue, Manhattan, NY, USA*
[3]*Department of Astronomy, Columbia University, Manhattan, NY, USA*

ABSTRACT

Gyrochronology, the method of inferring the age of a star from its rotation period, could provide ages for billions of stars over the coming decade of time-domain astronomy. However, the gyrochronology relations remain poorly calibrated due to a lack of precise ages for old, cool main-sequence stars. Now however, with proper motion measurements from Gaia, Galactic kinematics can be used as an age proxy, and the magnetic and rotational evolution of stars can be examined in detail. We demonstrate that kinematic ages, inferred from the velocity dispersions of groups of stars, beautifully illustrate the time and mass-dependence of the gyrochronology relations. We use the kinematic ages of field stars, plus benchmark clusters and asteroseismic stars, to calibrate a new empirical Gaussian process gyrochronology relation, that fully captures the complex rotational evolution of cool dwarfs over a range of masses and ages. We use cross validation to demonstrate that this relation accurately predicts ages for GKM dwarfs.

Keywords: Stellar Rotation — Stellar Evolution — Stellar Activity — Stellar Magnetic Fields — Low Mass Stars — Solar Analogs — Milky Way Dynamics

1. INTRODUCTION

Low mass dwarfs are the most common stars in the Milky Way, and their ages could reveal the evolution of Galactic stellar populations and planetary systems. However, the ages of GKM stars are difficult to measure because their luminosities and temperatures evolve slowly on the main sequence. Fortunately, rotation-dating, or 'gyrochronology' provides a promising means to measure precise ages for these cool dwarfs. (*e.g.* Schatzman 1962; Weber & Davis 1967; Kraft 1967; Skumanich 1972; Kawaler 1988; Pinsonneault et al. 1989; Barnes 2003, 2007; Mamajek & Hillenbrand 2008; Barnes 2010; Meibom et al. 2011, 2015; van Saders et al. 2016). The rotation periods of GKM stars evolve relatively rapidly, and a fully calibrated gyrochronology model that captures the time and mass-dependence of stellar spin down could provide ages that are precise to within 20% for millions of Milky Way stars in the time-domain era (Epstein & Pinsonneault 2014; Najita et al. 2016; Angus et al. 2019). However, gyrochronology models are not yet reliably calibrated, especially for low-mass and old stars.

A lack of low-mass and old calibration stars has previously limited the mass and age coverage of gyrochronology relations, which require precise age and rotation period measurements. Historically the calibration sample has been limited to open clusters and asteroseismic stars, which can be precisely dated with isochrone fitting and main sequence turn off, or precise oscillation frequency analysis. The rotation periods of both cluster and asteroseismic stars can be measured with precise time-series photometry. Magnetically active regions create inhomogeneous surface features and produce periodic variability in their integrated, broad-band emission. The photometric rotation periods of thousands of stars have been measured with the *Kepler/K2* and *TESS* space missions (Borucki et al. 2010; Howell et al. 2014; Ricker et al. 2015).

For the purposes of calibrating gyrochronology, open clusters provide good mass coverage for young stars: rotation periods have been measured for F to mid M dwarfs up to ages of around 700 Myr. In contrast, asteroseismic stars provide reasonable age coverage for hot stars: ages and photometric surface rotation periods have been measured for F, G and early K dwarfs up to ages of 10 Gyr. However, neither asteroseismology nor cluster analysis can provide rotation periods and ages for old, late K and M dwarfs. In addition, cluster and asteroseismic stars generally provide sparse coverage of the rotation period-effective temperature plane, and cannot reveal the detailed evolution of stellar

rotation rates. As a result, most empirical gyrochronology relations are only reliable for G dwarfs up to Solar age, K dwarfs up to 2-3 Gyr, and early M dwarfs up to < 1 Gyr.

The rotational evolution of cool dwarfs is not well understood because few old M dwarfs with rotation periods have age measurements. However, as we showed in Angus *et al.* (2020), the *kinematic* ages of field stars observed by *Kepler*, can provide a calibration sample with broad mass and age coverage. Although the *Kepler* sample does not include late M dwarfs, it can still be used to extend gyrochronology relations to much older ages for late K and early M dwarfs. By adding the ages and rotation periods of thousands of field stars to the open cluster and asteroseismic calibration sample, we can calibrate a gyrochronology relation that is applicable to FGK and early M dwarfs between the ages of ∼500 Myr and 8 Gyr.

1.1. *Core-envelope decoupling*

In Angus *et al.* (2020) we demonstrated that Galactic kinematics can be used to explore the evolution of stellar rotation. We showed that velocity dispersion, an established age proxy in the Galactic thin disk, increases smoothly as a function of rotation period, indicating that rotation period increases with age as expected. Using velocity dispersion as an age proxy, we also showed that old K dwarfs spin down more slowly than G dwarfs: their rotational evolution appears to 'stall' after around 1 Gyr, in a manner that reflects the behavior of K dwarfs observed in open clusters (Curtis et al. 2019). At young ages ($\sim 0.5 - 1$ Gyr), K dwarfs spin more slowly than G dwarfs of the same age, because their deeper convection zones generate stronger magnetic fields, which leads to more efficient magnetic braking. However, at old ages ($\gtrsim 1$ Gyr) K dwarfs rotate at the same rate or more rapidly than contemporary G dwarfs. The leading explanation for this phenomenon is that angular momentum is transferred from the core to the surface over longer timescales for lower-mass stars (Spada & Lanzafame 2019), *i.e.* they experience a more extended phase of 'core-envelope decoupling'.

A period of core-envelope decoupling is necessary to explain the observed rotation periods of stars in extremely young open clusters (1-10 Gyr) (*e.g.* Irwin et al. 2007; Bouvier 2008; Denissenkov et al. 2010; Spada et al. 2011; Reiners & Mohanty 2012; Gallet & Bouvier 2013). During this phase there is little transfer of angular momentum between radiative core and convective envelope and, as wind-braking removes angular momentum from the envelope, it decelerates while the core continues to spin rapidly. Over time however, angular momentum is transported across the interface between the two zones, and momentum from the rapidly spinning interior surfaces, inhibiting the deceleration of the outer envelope. Currently, the rotation periods of field and cluster stars can only be reproduced by semi-empirical models with a mass-dependent timescale for core-envelope coupling (Spada & Lanzafame 2019; Curtis et al. 2019, Angus *et al.*, 2020).

1.2. *Using kinematics as an age proxy*

The star forming molecular gas clouds observed in the Milky Way have a low out-of-plane, or vertical, velocity (*e.g.* Stark & Brand 1989; Stark & Lee 2005; Aumer & Binney 2009; Martig et al. 2014; Aumer et al. 2016). In contrast, the vertical velocities of older stars are observed to be larger in magnitude on average (Strömberg 1946; Wielen 1977; Nordström et al. 2004; Holmberg et al. 2007, 2009; Aumer & Binney 2009; Casagrande et al. 2011; Ting & Rix 2019; Yu & Liu 2018). There are two possible explanations for this observed increase in velocity dispersion with age: either stars are born kinematically 'cool' and their orbits are heated over time via interactions with giant molecular clouds (see Sellwood 2014, for a review of secular evolution in the MW), or stars formed kinematically 'hotter' in the past (*e.g.* Bird et al. 2013). Either way, the vertical velocity dispersions of thin disk stars are observed to increase with stellar age. This behavior is codified by Age-Velocity dispersion Relations (AVRs), which typically express the relationship between age and velocity dispersion as a power law: $\sigma_v \propto t^{\beta}$, with free parameter, β (*e.g.* Holmberg et al. 2009; Yu & Liu 2018). These expressions can be used to infer the ages of groups of stars from their velocity dispersions, as we do in this paper (see section **??**).

Kinematic ages have been used to explore the evolution of cool dwarfs for over a decade. West et al. (2004, 2006) found that the fraction of magnetically active M dwarfs decreases over time, by using the vertical distances of stars from the Galactic mid-plane as an age proxy, and West et al. (2008) used kinematic ages to calculate the expected activity lifetime for M dwarfs of different spectral types. Faherty et al. (2009) used tangential velocities to infer the ages of M, L and T dwarfs, and showed that dwarfs with lower surface gravities tended to be kinematically younger, and Kiman et al. (2019) used velocity dispersion as an age proxy to explore the evolution of Hα equivalent width (a magnetic activity indicator), in M dwarfs.

AVRs are usually calibrated in Galactocentric velocity coordinates ($v_{\mathbf{x}}$, $v_{\mathbf{y}}$, $v_{\mathbf{z}}$ or UVW), and these velocities can only be calculated with full 6D positional and velocity information, however most *Kepler* rotators do not have RV measurements[1]. In Angus *et al.* (2020) we used velocity in the direction of Galactic latitude ($v_{\mathbf{b}}$) as a stand-in for $v_{\mathbf{z}}$ because, in the *Galactic* coordinate system, velocities can be calculated from 3D positions and *2D* proper motions. The *Kepler* field lies at low Galactic latitude, so $v_{\mathbf{b}}$ is a close approximation to $v_{\mathbf{z}}$. Though $v_{\mathbf{b}}$ velocity dispersion does not equal $v_{\mathbf{z}}$ velocity dispersion, it still increases monotonically over time and provides accurate age rankings for *Kepler* stars. Unfortunately however, given that AVRs are calibrated in *Galactocentric* coordinates ($v_{\mathbf{x}}$, $v_{\mathbf{y}}$, $v_{\mathbf{z}}$), we could not directly translate $v_{\mathbf{b}}$ velocity dispersions to ages.

In this paper, our aim was to use kinematic ages to calibrate a new gyrochronology relation, for which four main steps were required. Firstly, we inferred *vertical* velocity, $v_{\mathbf{z}}$, for each star without an RV measurement by marginalizing over missing RVs using a hierarchical Bayesian model (see section **??**). Secondly, we calculated velocity dispersion for every star using a moving, or rolling dispersion method (see section **??**). Thirdly, these velocity dispersions were converted into ages using an AVR (Yu & Liu 2018, section **??**). Finally, we used a Gaussian process model to capture the complexities of stellar rotational evolution and calibrated a new gyrochronology relation using our kinematic ages, plus benchmark cluster and asteroseismic stars in section **??**.

[1] Although RVs for most will be released in *Gaia* DR3

2. DATA

This study focuses on stellar rotation in the original *Kepler* field. This is partly because *Kepler* provides the largest sample of published, homogeneously measured rotation periods, and partly because its low Galactic latitude allows us to marginalize over missing RV measurements and approximate vertical velocity, $v_{\mathbf{z}}$.

We combined two large rotation period catalogs constructed from original *Kepler* data, from McQuillan et al. (2014) and Santos et al. (2019). These two studies used different techniques to measure rotation periods from *Kepler* light curves: autocorrelation functions and wavelets respectively. The Santos et al. (2019) study was specifically focused on cooler stars: K and M dwarfs, and includes a larger number of rotation periods for these stars. The combined catalogs provide a total of over 38,000 rotation periods.

We used the publicly available *Kepler*-*Gaia* DR2 crossmatched catalog[2] to combine the McQuillan et al. (2014) and Santos et al. (2019) rotation catalogs with the *Gaia* DR2 catalog of parallaxes, proper motions and apparent magnitudes. Reddening and extinction from dust was calculated for each star using the Bayestar dust map implemented in the `dustmaps` *Python* package (M. Green 2018), and `astropy` (Astropy Collaboration et al. 2013; Price-Whelan et al. 2018). We used *Gaia* DR2 photometric color, $G_{\rm BP} - G_{\rm RP}$, to estimate effective temperatures for the stars in our sample, using the calibration in **?**.

Photometric binaries and subgiants were removed from the sample by applying cuts to the color-magnitude diagram (CMD), shown in figure **??**. A 6th-order polynomial was fit to the main sequence and raised by 0.27 dex to approximate the division between single stars and photometric binaries (shown as the curved dashed line in figure **??**). All stars above this line were removed from the sample. Potential subgiants were also removed by eliminating stars brighter than 4th absolute magnitude in *Gaia* G-band. This cut also removed a number of main sequence F stars from our sample, however these hot stars are not the focus of our gyrochronology study since their small convective zones inhibit the generation of a strong magnetic field. The removal of photometric binaries and evolved/hot stars reduced the total sample of around 38,000 stars by around 4,000.

Gaia DR2 provided RV measurements for 3587 stars in our sample, with a median uncertainty of 1.88 $\rm kms^{-1}$. RV measurements in *Gaia* DR2 were provided for stars with *Gaia* apparent magnitudes between around 4th and 13th, and 3550 K $\lesssim T_{\rm eff} \gtrsim$ 6900 K (Gaia Collaboration et al. 2018). We also crossmatched the McQuillan et al. (2014) sample with the 5th *LAMOST* data release (Cui et al. 2012; Xiang et al. 2019), adding a further 7466 RV measurements to the sample, and expanding the total number of stars with measured RVs to 11,053. The median uncertainty of the *LAMOST* RV measurements is 4.71 $\rm kms^{-1}$. Given that the *Gaia* RVs were more precise, on average, than the *LAMOST* RVs, we adopted the *Gaia* value in cases where both were available. *Gaia* DR3 will contain a large number of new RV measurements for stars in our sample.

To calculate kinematic ages, an estimate of vertical velocity, $v_{\mathbf{z}}$, is required. The ideal way to calculated $v_{\mathbf{z}}$ and similarly, $v_{\mathbf{x}}$ and $v_{\mathbf{y}}$, is to use 6D positional and velocity information. Many stars in the *Kepler* field do not have RV measurements and an alternative approach must be taken to infer their vertical velocities (see section **??**). However, a large number of *Kepler* rotators, over 10,000 of 34,000 *do* have RV measurements from *Gaia* DR2 and *LAMOST*. Figure **??** shows rotation period vs effective temperature for all stars in the McQuillan et al. (2014) and Santos et al. (2019) catalogs, plotted in grey. Stars with RV measurements are colored by their vertical velocity dispersion (see section **??** to see how we calculated velocity dispersion). Discuss what this plot shows.

Although RVs are available for a significant number of *Kepler* rotators (almost one in three), few stars cooler than 4000 K have RV measurements. This is due to the faint limits of the *Gaia* DR2 and *LAMOST* surveys (although RV measurements for fainter targets will be available in *Gaia* DR3). Given that magneto-rotational evolution is poorly understood for M dwarfs, the cool stars with missing RVs are arguably the ones we care most about. For this reason, we attempted to compensate for the lack of RV measurements by inferring vertical velocities for stars without RVs, to fill in the low-temperature region of figure **??** in section **??**.

[2] Available at gaia-kepler.fun

Figure 1. Vertical velocity dispersion as a function of rotation period and effective temperature for *Kepler* stars with measured rotation periods. Colored points show stars with RV measurements from *Gaia* or *LAMOST*, with their color indicating their velocity dispersion. Faint grey points show the combined McQuillan et al. (2014) and Santos et al. (2019) samples, including stars without RV measurements. The coolest stars in this sample do not have RVs because they are faint.

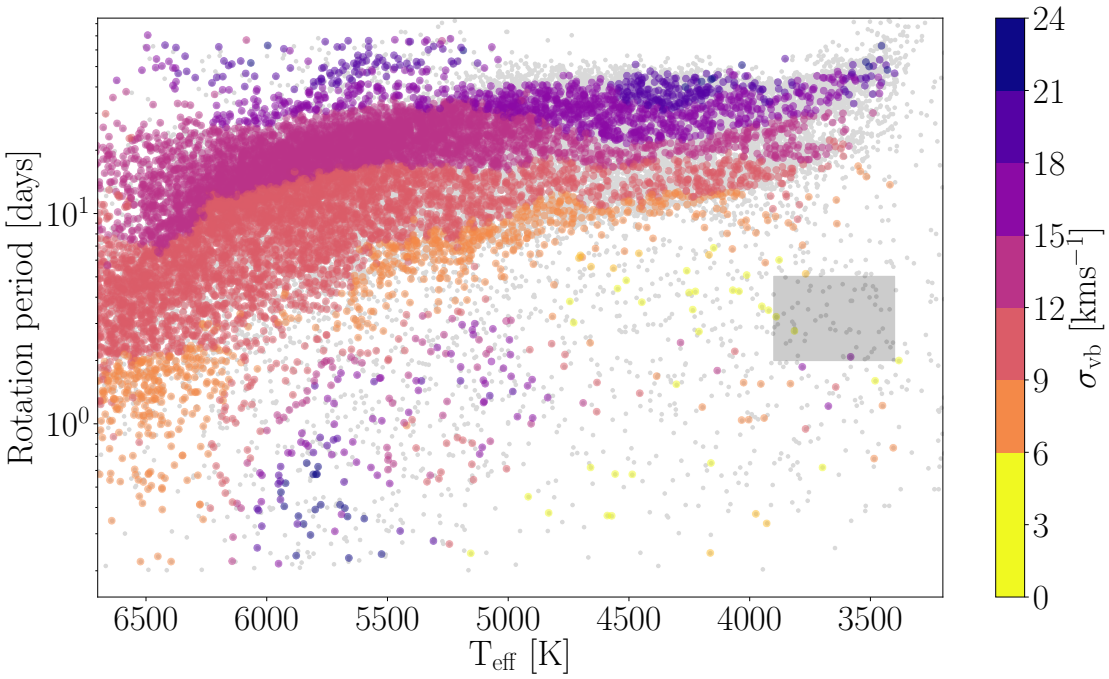

3. INFERRING 3D VELOCITIES (MARGINALIZING OVER MISSING RV MEASUREMENTS)

It has been demonstrated that the dispersion in vertical velocity, $v_{\mathbf{z}}$ for a group of stars increases with the age of that group (citations). However, velocities in Galactocentric coordinates, $v_{\mathbf{x}}$, $v_{\mathbf{y}}$ and $v_{\mathbf{z}}$, can only be calculated with full 6-D position and velocity information, *i.e.* proper motions, position and radial velocity. In Angus *et al.* (2020) we showed that kinematic ages can be used to explore rotational evolution and showed, in the appendix of that paper, that velocity, $v_{\mathbf{b}}$ in the Galactic frame, which can be calculated without an RV measurement, can be used as an approximation to $v_{\mathbf{z}}$ for *Kepler* stars. This is because the *Kepler* field of view lies at relatively low Galactic latitudes, ($\sim 5-20°$), so the z-direction is similar to the b-direction for *Kepler* stars. However, $v_{\mathbf{b}}$ is only a close approximation to $v_{\mathbf{z}}$ at extremely *low* latitudes, and even in the *Kepler* field, kinematic ages calculated with $v_{\mathbf{b}}$ instead of $v_{\mathbf{z}}$ are systematically larger because of extra noise introduced by the imperfect translation between $v_{\mathbf{b}}$ and $v_{\mathbf{z}}$. In this work, we *infer* $v_{\mathbf{z}}$ by marginalizing over missing RV measurements.

For each star in our sample, we inferred $v_{\mathbf{x}}$, $v_{\mathbf{y}}$, and $v_{\mathbf{z}}$ from the 3D positions and 2D proper motions provided in the *Gaia* DR2 catalog (Brown et al. 2011). We also simultaneously inferred distance, (instead of using inverse-parallax), to model velocities (see *e.g.* Bailer-Jones 2015; Bailer-Jones et al. 2018).

Using Bayes rule, the posterior probability of the parameters given the data can be written:

$$p(v_{\mathbf{xyz}}, D|\mu_\alpha, \mu_\delta, \alpha, \delta, \pi) = p(\mu_\alpha, \mu_\delta, \alpha, \delta, \pi|v_{\mathbf{xyz}}, D)p(v_{\mathbf{xyz}})p(D), \quad (1)$$

where D is distance, α is Right Ascension (RA), δ is declination (dec), π is parallax, μ_α is proper motion in RA, and μ_δ is proper motion in dec.

For each star in the *Kepler* field, we explored the posteriors of these four parameters using the *PyMC3* Hamiltonion Monte Carlo (HMC) sampler (citations).

3.1. *The prior*

- **Why is the prior important?** Arguably, the trickiest part of this inference is in selecting an appropriate prior. Stellar velocities (in certain directions), inferred without RV measurements may be sensitive to the prior.

- **How we calculated the prior.** We used the mean and covariance of the distance and velocity distributions of *Kepler* targets *with* RV measurements to determine the 4D multivariate Gaussian prior over log(distance) and velocities. 3D velocities were calculated for every star with an RV measurement from either *Gaia* or *LAMOST*. These velocities were then sigma-clipped at the 3-sigma level in all three dimensions to remove large velocity outliers which may be caused by proper motion or RV measurements with large errors. We then calculated the mean and covariance of the multivariate Gaussian distribution of $v_{\mathbf{x}}$, $v_{\mathbf{y}}$, $v_{\mathbf{z}}$, and ln(Distance). We used this mean and covariance to construct our multivariate Gaussian prior.

- **Is is important to select the prior carefully.** Our goal was to infer the velocities of stars without RV measurements using a prior calculated from stars *with* RV measurements. However, stars with and without RVs are likely to be slightly different populations, the parameters of which depend on the *Gaia* and *LAMOST* selection function. Discuss selection functions. In particular, stars without RV measurements are more likely to be faint, and therefore, less massive. Lower-mass stars are, on average, older, and have larger velocity dispersions. So a prior based on the velocity distributions of stars with RVs will not necessarily reflect the velocities of those without.

- **Testing the prior.** For this reason, we tested how the choice of prior affected the velocities we inferred. We tested two priors: one calculated from the velocity distributions of the brightest half of the RV sample (*Gaia* G-band apparent magnitude < 13.9), and one from the faintest half ($G > 13.9$). We selected the 500 faintest stars from the *Gaia-LAMOST* RV sample to test these two priors on. We chose the faintest stars as these are the most likely to be similar to the non-RV sample, and to enlarge the difference between the bright prior and the test sample. The results of this test are shown in figure **??**

- **Although the prior isn't perfect, it's good enough for our study.**

We tuned the *PyMC3* model for 1500 steps, with a target acceptance fraction of 0.9. The model was then run for 1000 steps with 4 chains.

Figure 2.

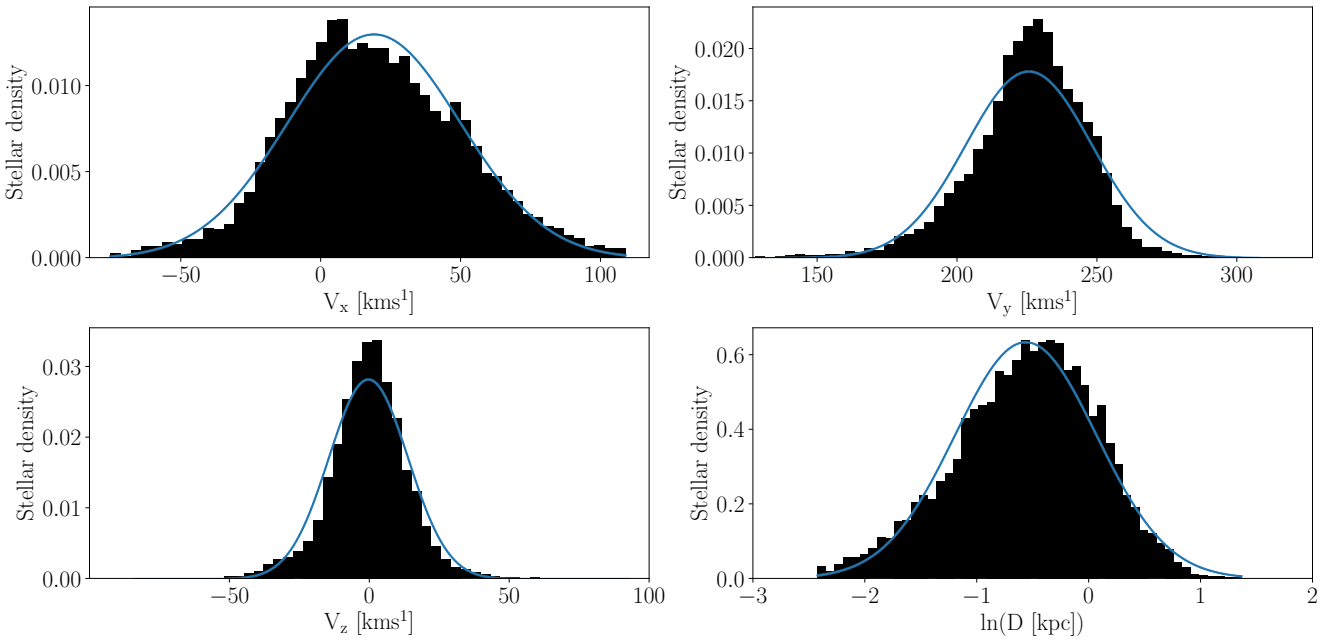

Figure 3. Vertical velocities calculated with full 6D information vs vertical velocities inferred without RV, for all 3000 McQuillan et al. (2014) stars with *Gaia* RV measurements.

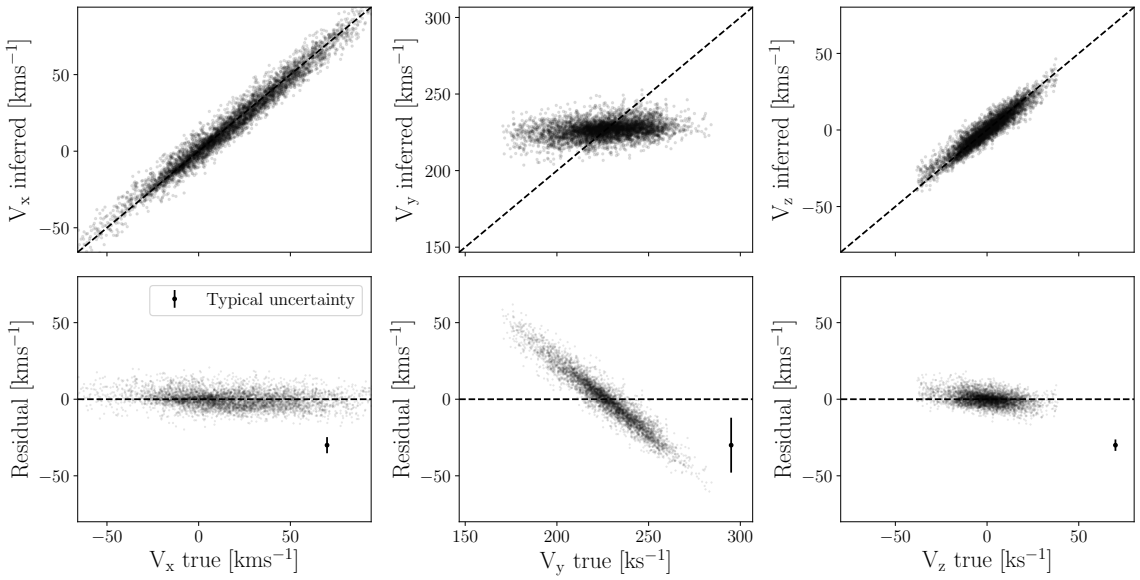

Figure **??** shows the $v_{\mathbf{x}}$, $v_{\mathbf{y}}$ and $v_{\mathbf{z}}$ velocities we inferred, compared with those calculated from measured RVs. 2000 stars are shown, which were chosen at random from the *Kepler* rotators with RV measurements. The *Kepler* field is oriented almost along the **y**axis of the Galactocentric coordinate system. As a result, **x** and **z**-direction velocities of *Kepler* stars are extremely well-constrained with proper motion alone, but $v_{\mathbf{y}}$ is almost completely unconstrained

without an RV. Figure **??** shows that $v_{\mathbf{x}}$ and $v_{\mathbf{z}}$ velocities inferred without RV measurements are extremely similar to those calculated with RVs.

4. KINEMATIC AGES

4.1. *Calculating velocity dispersions*

A kinematic age can be calculated from the velocity dispersion, *i.e.* standard deviation, of a group of stars. These velocity dispersions can then be converted into an age using an AVR (*e.g.* Holmberg et al. 2009; Yu & Liu 2018). Kinematic ages represent the *average age* of a group of stars and are most informative when stars are grouped by age. If a group of stars have similar ages, their kinematic age will be close the age of each individual. On the other hand, the kinematic age of a group with large age variance will not provide much information about the ages of individual stars. Velocity distributions themselves do not reveal whether a group of stars have similar or different ages, since either case the velocities are Gaussian-distributed. Fortunately however, we can group *Kepler* stars by age using the implicit assumption that underpins gyrochronology: that stars with the same rotation period and color are the same age. We discuss the implications of this assumption and cases where it doesn't apply in the Discussion of this paper (section **??**).

In this paper, we calculated the kinematic age of *each individual star* in our sample, by grouping it with its neighbors in $\log(P_{\rm rot})$–$T_{\rm eff}$ space. This method is similar to calculating a rolling, or running standard deviation and allowed us to assign a unique age to each star. However, ages calculated this way are tightly correlated, and their correlation depends strongly on window-size.

We tested two methods of grouping stars: K-nearest neighbors, and bins in $\log(P_{\rm rot})$ and $T_{\rm eff}$. In the K-nearest neighbors method, each star was grouped with the K-nearest stars in $\log(P_{\rm rot})$-$T_{\rm eff}$ space. Groups created this way spanned a small $\log(P_{\rm rot})$-$T_{\rm eff}$ range where the stellar number density was large, and a large range where the number density was small. In other words, the number of stars was fixed but the window-size changed. In the fixed range method, stars were grouped within a fixed $\log(P_{\rm rot})$-$T_{\rm eff}$window. This method created groups with large numbers of stars in densely populated regions of the $\log(P_{\rm rot})$–$T_{\rm eff}$ plane, and small numbers of stars in sparsely populated regions, *i.e.* the number of stars changed but the window-size was fixed. To choose the best method, and to optimize for the parameters of each (K and window-size), we conducted a set of tests.

4.2. *Converting velocity dispersion to age with an AVR*

We used the Yu & Liu (2018) AVR to convert velocity dispersion to age. This relation was calibrated using the ages and velocities of red clump stars. They divided their sample into metal rich and poor subsets, and calibrated separate AVRs for each, plus a global AVR. Their AVR is a power law:

$$\sigma_{vz} = \alpha t^{\beta}, \tag{2}$$

where α and β take values (6.38, 0.578) for metal rich stars (3.89, 1.01) for metal poor stars, and (5.47, 0.765) for all stars.

We used 1.5× the Median Absolute Deviation (MAD) of velocities, which is a robust approximation to the standard deviation and is less sensitive to outliers. Velocity outliers could be binary stars or could be generated by underestimated parallax or proper motion uncertainties.

4.3. *Comparing kinematic ages with asteroseismic and cluster ages*

4.4. *A Gaussian process gyrochronology relation*

6. DISCUSSION

7. CONCLUSION

This work was partly developed at the 2019 KITP conference 'Better stars, better planets'. Parts of this project are based on ideas explored at the Gaia sprints at the Flatiron Institute in New York City, 2016 and MPIA, Heidelberg, 2017. This work made use of the gaia-kepler.fun crossmatch database created by Megan Bedell.

Some of the data presented in this paper were obtained from the Mikulski Archive for Space Telescopes (MAST). STScI is operated by the Association of Universities for Research in Astronomy, Inc., under NASA contract NAS5-26555. Support for MAST for non-HST data is provided by the NASA Office of Space Science via grant NNX09AF08G and by other grants and contracts. This paper includes data collected by the Kepler mission. Funding for the *Kepler* mission is provided by the NASA Science Mission directorate.

This work has made use of data from the European Space Agency (ESA) mission *Gaia* (https://www.cosmos.esa.int/gaia), processed by the *Gaia* Data Processing and Analysis Consortium (DPAC, https://www.cosmos.esa.int/web/gaia/dpac/consortium). Funding for the DPAC has been provided by national institutions, in particular the institutions participating in the *Gaia* Multilateral Agreement.

REFERENCES

Angus, R., Morton, T. D., & Foreman-Mackey *et al*, D. 2019, AJ, 158, 173, doi: 10.3847/1538-3881/ab3c53

Astropy Collaboration, Robitaille, T. P., & Tollerud *et al*, E. J. 2013, A&A, 558, A33, doi: 10.1051/0004-6361/201322068

Aumer, M., Binney, J., & Schönrich, R. 2016, MNRAS, 462, 1697, doi: 10.1093/mnras/stw1639

Aumer, M., & Binney, J. J. 2009, MNRAS, 397, 1286, doi: 10.1111/j.1365-2966.2009.15053.x

Bailer-Jones, C. A. L. 2015, PASP, 127, 994, doi: 10.1086/683116

Bailer-Jones, C. A. L., Rybizki, J., & Fouesneau *et al*, M. 2018, AJ, 156, 58, doi: 10.3847/1538-3881/aacb21

Barnes, S. A. 2003, ApJ, 586, 464, doi: 10.1086/367639

—. 2007, ApJ, 669, 1167, doi: 10.1086/519295

—. 2010, ApJ, 722, 222, doi: 10.1088/0004-637X/722/1/222

Bird, J. C., Kazantzidis, S., & Weinberg *et al*, D. H. 2013, ApJ, 773, 43, doi: 10.1088/0004-637X/773/1/43

Borucki, W. J., Koch, D., & Basri *et al*, G. 2010, Science, 327, 977, doi: 10.1126/science.1185402

Bouvier, J. 2008, A&A, 489, L53, doi: 10.1051/0004-6361:200810574

Brown, T. M., Latham, D. W., & Everett *et al*, M. E. 2011, AJ, 142, 112, doi: 10.1088/0004-6256/142/4/112

Casagrande, L., Schönrich, R., & Asplund *et al*, M. 2011, A&A, 530, A138, doi: 10.1051/0004-6361/201016276

Cui, X.-Q., Zhao, Y.-H., & Chu *et al.*, Y.-Q. 2012, Research in Astronomy and Astrophysics, 12, 1197, doi: 10.1088/1674-4527/12/9/003

Curtis, J. L., Agüeros, M. A., & Douglas *et al*, S. 2019, arXiv e-prints. https://arxiv.org/abs/1905.06869

Denissenkov, P. A., Pinsonneault, M., & Terndrup *et al*, D. M. 2010, ApJ, 716, 1269, doi: 10.1088/0004-637X/716/2/1269

Epstein, C. R., & Pinsonneault, M. H. 2014, ApJ, 780, 159, doi: 10.1088/0004-637X/780/2/159

Faherty, J. K., Burgasser, A. J., & Cruz *et al*, K. L. 2009, AJ, 137, 1, doi: 10.1088/0004-6256/137/1/1

Gaia Collaboration, Brown, A. G. A., & Vallenari *et al.*, A. 2018, A&A, 616, A1, doi: 10.1051/0004-6361/201833051

Gallet, F., & Bouvier, J. 2013, A&A, 556, A36, doi: 10.1051/0004-6361/201321302

Holmberg, J., Nordström, B., & Andersen, J. 2007, A&A, 475, 519, doi: 10.1051/0004-6361:20077221

—. 2009, A&A, 501, 941, doi: 10.1051/0004-6361/200811191

Howell, S. B., Sobeck, C., & Haas *et al*, M. 2014, PASP, 126, 398, doi: 10.1086/676406

Irwin, J., Hodgkin, S., & Aigrain *et al*, S. 2007, MNRAS, 377, 741, doi: 10.1111/j.1365-2966.2007.11640.x

Kawaler, S. D. 1988, ApJ, 333, 236, doi: 10.1086/166740

Kiman, R., Schmidt, S. J., & Angus *et al*, R. 2019, AJ, 157, 231, doi: 10.3847/1538-3881/ab1753

Kraft, R. P. 1967, ApJ, 150, 551, doi: 10.1086/149359

M. Green, G. 2018, The Journal of Open Source Software, 3, 695, doi: 10.21105/joss.00695

Mamajek, E. E., & Hillenbrand, L. A. 2008, ApJ, 687, 1264, doi: 10.1086/591785

Martig, M., Minchev, I., & Flynn, C. 2014, MNRAS, 443, 2452, doi: 10.1093/mnras/stu1322

McQuillan, A., Mazeh, T., & Aigrain, S. 2014, ApJS, 211, 24, doi: 10.1088/0067-0049/211/2/24

Meibom, S., Barnes, S. A., & Latham *et al*, D. W. 2011, ApJL, 733, L9, doi: 10.1088/2041-8205/733/1/L9

Meibom, S., Barnes, S. A., & Platais *et al*, I. 2015, Nature, 517, 589, doi: 10.1038/nature14118

Najita, J., Willman, B., & Finkbeiner *et al*, D. P. 2016, arXiv e-prints, arXiv:1610.01661. https://arxiv.org/abs/1610.01661

Nordström, B., Mayor, M., & Andersen *et al*, J. 2004, A&A, 418, 989, doi: 10.1051/0004-6361:20035959

Pinsonneault, M. H., Kawaler, S. D., & Sofia *et al*, S. 1989, ApJ, 338, 424, doi: 10.1086/167210

Price-Whelan, A. M., Sipőcz, B. M., & Günther *et al*, H. M. 2018, AJ, 156, 123, doi: 10.3847/1538-3881/aabc4f

Reiners, A., & Mohanty, S. 2012, ApJ, 746, 43, doi: 10.1088/0004-637X/746/1/43

Ricker, G. R., Winn, J. N., & Vanderspek *et al*, R. 2015, Journal of Astronomical Telescopes, Instruments, and Systems, 1, 014003, doi: 10.1117/1.JATIS.1.1.014003

Santos, A. R. G., García, R. A., & Mathur *et al*, S. 2019, ApJS, 244, 21, doi: 10.3847/1538-4365/ab3b56

Schatzman, E. 1962, Annales d'Astrophysique, 25, 18

Sellwood, J. A. 2014, Reviews of Modern Physics, 86, 1, doi: 10.1103/RevModPhys.86.1

Skumanich, A. 1972, ApJ, 171, 565, doi: 10.1086/151310

Spada, F., & Lanzafame, A. C. 2019, arXiv e-prints, arXiv:1908.00345. https://arxiv.org/abs/1908.00345

Spada, F., Lanzafame, A. C., & Lanza *et al*, A. F. 2011, MNRAS, 416, 447, doi: 10.1111/j.1365-2966.2011.19052.x

Stark, A. A., & Brand, J. 1989, ApJ, 339, 763, doi: 10.1086/167334

Stark, A. A., & Lee, Y. 2005, ApJL, 619, L159, doi: 10.1086/427936

Strömberg, G. 1946, ApJ, 104, 12, doi: 10.1086/144830

Ting, Y.-S., & Rix, H.-W. 2019, ApJ, 878, 21, doi: 10.3847/1538-4357/ab1ea5

van Saders, J. L., Ceillier, T., & Metcalfe *et al*, T. S. 2016, Nature, 529, 181, doi: 10.1038/nature16168

Weber, E. J., & Davis, Jr., L. 1967, ApJ, 148, 217, doi: 10.1086/149138

West, A. A., Bochanski, J. J., & Hawley *et al*, S. L. 2006, AJ, 132, 2507, doi: 10.1086/508652

West, A. A., Hawley, S. L., & Bochanski *et al*, J. J. 2008, AJ, 135, 785, doi: 10.1088/0004-6256/135/3/785

West, A. A., Hawley, S. L., & Walkowicz *et al*, L. M. 2004, AJ, 128, 426, doi: 10.1086/421364

Wielen, R. 1977, A&A, 60, 263

Xiang, M., Ting, Y.-S., & Rix *et al.*, H.-W. 2019, ApJS, 245, 34, doi: 10.3847/1538-4365/ab5364

Yu, J., & Liu, C. 2018, MNRAS, 475, 1093, doi: 10.1093/mnras/stx3204